IET Renewable Power Generation

Special Issue Call for Papers

Be Seen. Be Cited.
Submit your work to a new IET special issue

Connect with researchers and experts in your field and share knowledge.

Be part of the latest research trends, faster.

Read more

The Institution of Engineering and Technology

Received: 28 February 2021 | Revised: 14 July 2021 | Accepted: 5 August 2021

DOI: 10.1049/rpg2.12277

IET Renewable Power Generation

The Institution of Engineering and Technology WILEY

ORIGINAL RESEARCH PAPER

Power absorption modelling and analysis of a multi-axis wave energy converter

Ming Tan[1] | Yuhao Cen[1] | Yuxuan Yang[1] | Xiaodong Liu[1] | Yulin Si[1] | Peng Qian[1] | Dahai Zhang[1,2,3,4]

[1] Ocean College, Zhejiang University, Zhoushan 316021, China

[2] State Key Laboratory of Fluid Power and Mechatronic Systems, Zhejiang University, Hangzhou 310027, China

[3] Hainan Institute of Zhejiang University, Sanya 572025, P. R. China

[4] The Engineering Research Center of Oceanic Sensing Technology and Equipment, Ministry of Education, Zhoushan, China

Correspondence
Dahai Zhang, Institute of Ocean Engineering and Technology, Ocean College, Zhejiang University, Zhoushan, 316021, China.
Email: zhangdahai@zju.edu.cn

Funding information
Ministry of Science and Technology of the People's Republic of China, Grant/Award Number: 2018YFB1501900; Zhejiang Provincial Department of Science and Technology, Grant/Award Number: 2021C03182; National Natural Science Foundation of China, Grant/Award Number: 51879233; Natural Science Foundation of Zhejiang Province, Grant/Award Number: LHY20E090001; Bureau of Science and Technology of Zhoushan, Grant/Award Numbers: 2019C81036, 2021C81001; Fundamental Research Funds for the Central Universities

Abstract

A point absorber wave energy converter (WEC) which converts wave energy into electrical energy with a multi-axis power-take-off (PTO) system is considered here. Previous wave tank trials have proved the ability of the multi-axis WEC to absorb wave power. In this study, the boundary element method (BEM) based software Ansys@ AQWA™ was applied to model and analyze the power absorption performance of the multi-axis WEC for a wider range of regular and irregular waves. To verify the numerical model, a laboratory-scale physical model was manufactured and tested. Results show that the multi-axis WEC can absorb more power from the incident regular wave power compared to single-axis WECs and the efficiency reaches up to 45%. It is found that the wave frequency and incident angle significantly influence the amount of absorbed power from different motion modes and PTO axes. Then the numerical model is simulated at 12 nearshore locations in East and South China Sea. The results indicate that the multi-axis WEC can absorb up to 5 kW and the efficiency can reach up to 29% at the most energetic site Shengshan. In addition, considerable differences of mean absorbed power efficiency can be found between sea states.

1 | INTRODUCTION

In the last few decades, a wide variety of wave energy technologies based on different working principles was proposed and developed. Recent reviews can be found in [1]. Among them, point absorber WECs that possess small dimensions relative to the incident wavelength are particularly popular due to their simpler structure, easier maintenance, and better suitability for deep-sea deployment. An early example was the device named Norwegian buoy developed by Norwegian researchers which was tested in the Trondheim Fjord in 1983 [2]. There are several other famous devices like Wavebob [3], PowerBuoy [4], Archimedes Wave Swing (AWS [5]), PS Frog [6] and so on. The power in ocean waves is composed of kinetic and potential energy moving in multiple directions. Unfortunately, most of the point absorber WECs are single-axis devices and extract energy from one direction of motion. In the ideal case, a point absorber WEC can convert all the usable energy of ocean waves to electricity by oscillating freely in six motion modes meaning that a multi-axis device should be able to generate more electricity than most single-axis devices.

The present work aims at studying a point absorber WEC which can convert wave energy into electrical energy through a three-axis PTO system composed of one translational axis and

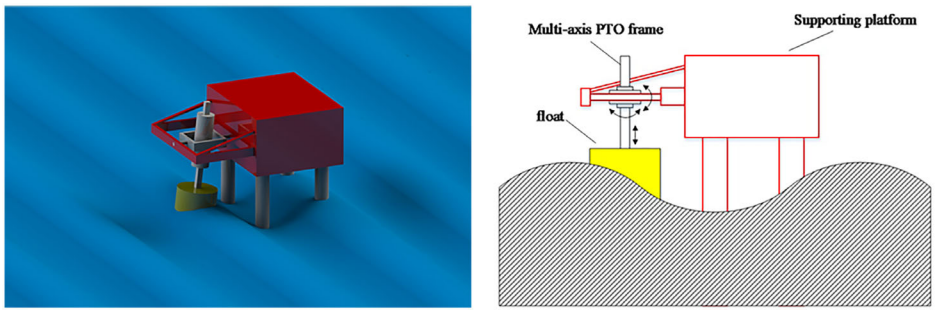

FIGURE 1 Concept of the multi-axis WEC

two rotational axes (Figure 1). The capability of the device to harness wave energy has been demonstrated through previous wave tank series and its ability to absorb up to 40% of the incident wave energy was proved [7, 8]. At present, this work aims to design the certain scaled multi-axis WEC specially tailored for the Zhejiang and Guangdong nearshore sea states in East and South China Sea and it is promising to advance it to the next stage.

Compared to the traditional single-axis PTO point absorber WECs, studies on the multi-axis WECs are relatively insufficient and less systematic. It is worth noting that the most important reason for the wide use of single-axis WECs rather than multi-axis WECs is that increasing number of degree of freedom (DOF) of systems would result in the interaction between modes of buoy's motion and power absorption along different PTO axes which introduce difficulties into modelling and simulation studies. A multi-axis PTO system means a more complicated mechanism and the responses of every PTO axis always interact with each other. The time-varying displacement along each PTO axis is different and the wave force that acts on each PTO axis is also not the same. Power output along one axis can even become the load of the others. Some of these complexities have been reported in [9], where the control strategies and power optimization of a 2-DOF WEC were addressed. Focusing on the power absorption in each PTO axis is a key issue aiming to illustrate the interference between each PTO axis. As a result, before taking the multi-axis WEC into next stage of research and application, inherent power absorption characteristics of multi-axis WECs compared to single-axis devices need to be deeply studied.

Considering these issues, numerical modelling becomes necessary to simulate the effects of additional PTO axes and investigate the power absorption performance of a multi-axis WEC. The major advantages of using numerical modelling are to test several WEC configurations and wave conditions at a lower cost than with experimental tests, though a simplified physical model test is needed to validate the results obtained with numerical models.

The methods on how to build numerical models of the WECs have been a hot issue of research so far. In recent years, an increasing number of numerical modelling techniques have been developed. Each of the WEC numerical modelling methods has a certain set of characteristics that makes it more or less suitable for a particular WEC. In recent years, BEM-based numerical codes such as the well-known WAMIT, Aquaplus and AQWA are commonly used to model the interactions between WECs and the incident waves. [10] studied the power performance of a two-body heave converter using time domain models. [11] investigated the influence of the shape, draft and diameter of the model on the power absorption by building frequency domain models with hydrodynamic parameters calculated in AQWA. [12] investigated the hydrodynamic performance of an oscillating water column WEC by using a higher order BEM. [13] carried out an extensive study of the influence of the PTO characteristics on the performance of CECO wave energy converter and concluded that the CECO WEC can absorb between 10% and 40% of the incident waves. Later, [14] presented a study on the effects of the direction of the translation motion on the power capture of the CECO WEC in AQWA. Although it brings the loss of accuracy and the increase in computational cost, the BEM is still the most recommended method for investigating the performance of large-scale WECs, especially the multi-DOF systems. It has been reported by [15, 16] that the time domain models are more suitable for studies on irregular waves and related non-linear forces and oscillations than frequency-domain models which suit regular waves and systems with linear approximations. In order to realistically investigate the performance of the multi-axis WEC, any further simulation works in this study will be carried out in time domain.

This work aims to obtain a detailed knowledge of the behaviour of the multi-axis WEC in terms of the following performance characteristics: the interaction between translation and rotation modes, the absorbed power and efficiency of the device and the differences of performance between modes. In order to achieve this, the performance of multi-axis WEC was simulated first in the time domain with AQWA for a wider number of regular wave conditions. In this study, the multi-axis WEC with a cylindrical buoy were considered, and two kinds of single-axis WEC were also analysed for comparison. Later, as an application case study, the mean power absorbed by the multi-axis WEC at the 12 Zhejiang and Guangdong nearshore locations in the East and South China Sea is estimated, as well as the power absorption efficiency.

This paper is organized as follows: In Section 2, a description of the multi-axis WEC design concepts, the mathematic model and the BEM model in AQWA are presented; Simulations for regular waves with different periods and heights are shown in Section 3, while the results are detailedly discussed including the analysis of the WEC performance characteristics; then, the application to real sea states in East and South China Sea

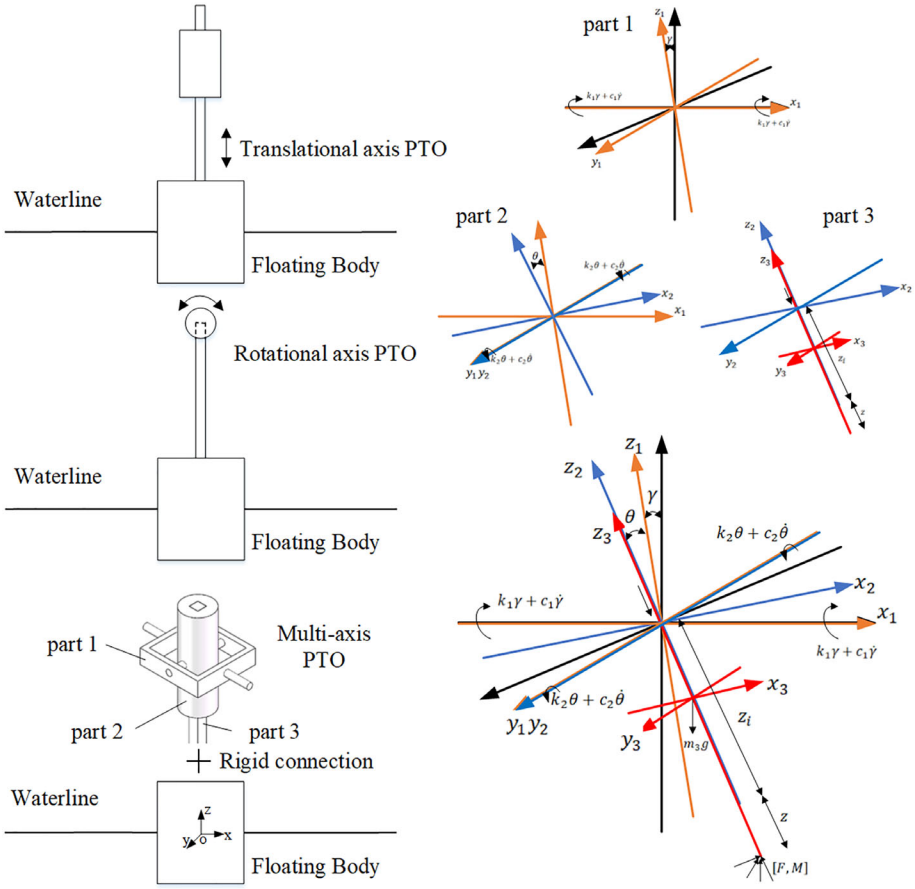

FIGURE 2 The schematic of WECs: (a) translation-axis WEC, (b) rotation-axis WEC, (c) multi-axis WEC

is presented in Section 4; Finally, the main conclusion and prospective work is mentioned in Section 5.

2 | MODEL AND METHODS

2.1 | Mathematic models

The simplified scheme of the multi-axis point absorber WEC is shown in Figure 2. A vertical cylinder is adopted as the geometry of the floating buoy, which introduces heave, pitch and roll oscillations. The proposed multi-axis PTO structure consists of a vertical shaft (part 3 in Figure 2) and a cylindrical linear bearing (part 2 in Figure 2) linked to a rectangular frame (part 1 in Figure 2) by means of two pairs of joints, allowing the buoy to move anywhere within the limits of the PTO system. For a multi-axis structure, there are three relative motions, that is, three modes of energy absorption, namely translation mode, two rotation modes (defined as rotational1 mode and rotational2 mode, respectively). Compared to traditional translational/rotational axis devices, two more axis PTO units were added making it possible to absorb both kinetic and potential energy. A linear damper in each joint of the device provides the conversion of the energy absorbed from waves. A major problem with this kind of application in real sea states is an offshore platform where the multi-axis PTO system being installed needs to be built. Another potential problem is that the complexity of supporting structure and PTO system mean higher costs and risks. A full discussion of reliability and economics problems lies beyond the scope of this study and will not be discussed here.

Two kinds of single-axis WECs are also demonstrated in Figure 2 as a comparison group. These single-axis WECs, commonly referred to as single translational axis or single rotational axis WECs, have been extensively studied [17, 18]. In this study, the same floating cylindrical buoy was also applied to the single-axis WECs. Such a choice has been made in order to compare the performance of single-axis WECs explicitly with the performance of the multi-axis WEC.

The dynamic analysis of the multi-axis device needs to be divided into two parts: the hydrodynamic interaction between floating buoy and waves, and the multi-body dynamics of multi-axis structure. For the hydrodynamic analysis, the equation of motion could be expressed in a convolution integral form:

$$\{m+A_{\infty}\}\ddot{X}(t)+c\dot{X}(t)+KX(t)+\int_0^t R(t-\omega)\dot{X}(\tau)d\omega = F(t), \quad (1)$$

where X(t) is the motion response of the buoy, m is the structure mass matrix, A_∞ is the fluid added mass matrix at infinite frequency, c is the damping matrix except the linear radiation damping effects due to diffraction panels, K is the total stiffness matrix, R(t) is the velocity impulse function matrix, and F(t) is the external force acting on the centre of gravity of the float.

In which R(t) and A_∞ are defined by:

$$R(t) = \frac{2}{\pi}\int_0^\infty B(\omega)\cos(\omega t)\,d\omega, \tag{2}$$

$$A_\infty = A(\omega) + \frac{1}{\omega}\int_0^\infty R(t)\sin(\omega t)\,d\omega, \tag{3}$$

where $A(\omega)$ and $B(\omega)$ are the added mass and hydrodynamic damping matrices, respectively.

The external force comprises three components:

$$F(t) = F_e(t) + F_{PTO}(t) + F_{cons}(t), \tag{4}$$

where the first term represents the wave excitation force on the body, the second refers to the reaction force from the PTO system and the third to the constraint force caused by the supporting frame to hold the WEC in position.

The coordinate system and several key parameters of the system need to be defined before carrying out and dynamic analysis [7]. Here, same definition of the coordinate system and method to derive the dynamic equation of motion is adopted, as shown in Figure 2. The global coordinates of the model are $(X, Y, Z)$and the local coordinates (x_1, y_1, z_1),(x_2, y_2, z_2), $(x_3, y_3, z_3)$are the coordinates for the individual motion components of the multi-axis WEC model, respectively—a rotational about the rotational1-axis (part 1), a rotational about the rotational2-axis (part 2) and a translation along the translational-axis (part 3), as shown in Figure 2. The input wave forces $[F, M]$ transmitted from the buoy act at the lower end of part 3 which is rigidly connected to the floating body.

The dynamic analysis of the multi-axis structure is similar to that of a gyroscope and thus the motion equation can be formulated by applying the Newton–Euler equations.

$$\begin{pmatrix} F \\ M \end{pmatrix} = \begin{pmatrix} mI & -m[c] \\ m[c] & J_c - m[c][c] \end{pmatrix} \begin{pmatrix} \ddot{r} \\ \ddot{\omega} \end{pmatrix} + \begin{pmatrix} m\omega \times (\omega \times c) \\ \omega \times (J_c - m[c][c])\,\omega \end{pmatrix}, \tag{5}$$

where F is the total force acting on the centre of gravity; M is the total moment acting about the centre of gravity; m is the mass of the body; $\ddot{r}$ and $\ddot{\omega}$ are the linear and angular acceleration of the system; J_c is the mass moment of inertia about the centre of mass; I is the identity matrix; c is the location of the centre of mass of the system in the global coordinate.

The dynamic equation of the multi-axis structure is obtained by applying Equation (5) to the system:

$$\begin{bmatrix} 0 \\ 0 \\ F_z - k_3 z(t) - c_3 \dot{z}(t) - m_3 g \cos\gamma(t)\cos\theta(t) \\ -2k_1\gamma(t) - 2c_1\dot{\gamma}(t) - m_3 g z_g \sin\gamma(t)\cos\theta(t) - M_y\left(z(t) + z_i + 1\right) - F_y\left(z(t) + z_i\right) \\ -2k_2\theta(t) - 2c_1\dot{\theta}(t) - m_3 g z_g \sin\theta(t) + M_x\left(z(t) + z_i + 1\right) + F_x\left(z(t) + z_i\right) \\ 0 \end{bmatrix}$$

$$= \begin{bmatrix} m_3 & 0 & 0 & 0 & m_3 z_g & 0 \\ 0 & m_3 & 0 & m_3 z_g & 0 & 0 \\ 0 & 0 & m_3 & 0 & 0 & 0 \\ 0 & -m_3 z_g & 0 & I_{xx} + m_3 z_g^2 & 0 & 0 \\ -m_3 z_g & 0 & 0 & 0 & I_{yy} + m_3 z_g^2 & 0 \\ 0 & 0 & 0 & 0 & 0 & I_{zz} \end{bmatrix} \begin{bmatrix} 0 \\ 0 \\ \ddot{z}(t) \\ \ddot{\gamma}(t) \\ \ddot{\theta}(t) \\ 0 \end{bmatrix}$$

$$+ \begin{bmatrix} 0 \\ 0 \\ \dot{\gamma}^2(t)\, m_3 z_g + \dot{\theta}^2(t)\, m_3 z_g \\ 0 \\ 0 \\ \dot{\gamma}(t)\dot{\theta}(t)\left(I_{xx} + m_3 z_g^2\right) - \dot{\gamma}(t)\dot{\theta}(t)\left(I_{yy} + m_3 z_g^2\right) \end{bmatrix} \tag{6}$$

where k_1, k_2 and k_3 are the stiffness of each joint and c_1, c_2 and c_3 are the damping constants of each joint, respectively. I_{xx}, I_{yy} are the moments of inertia of the system about the axes, z_g is the distance from the origin of the global coordinate to the centre of gravity of the system. γ, θ and z are the rotational displacements about the X-axis, Y-axis and linear displacement along the Z-axis, respectively, z_i is the distance between the origin of the global coordinate system and the buoy, and $m_3 g$ is the weight of the part 3. Each component in $[F_x\ F_y\ F_z, M_x\ M_y\ M_z]$ is decomposed by the input wave forces $[F, M]$.

The time-averaged absorbed power in each PTO axis can be calculated as:

$$P_\gamma = \frac{1}{T}\int_0^T c_1\dot{\gamma}^2(t)\,dt$$

$$P_\theta = \frac{1}{T}\int_0^T c_2\dot{\theta}^2(t)\,dt$$

$$P_z = \frac{1}{T}\int_0^T c_3 z^2(t)\,dt. \tag{7}$$

The time-averaged total absorbed power of the system is

$$P_{\text{total}} = P_{\gamma} + P_{\theta} + P_{z}. \tag{8}$$

A common parameter used to represent the performance of a point absorber WEC is the capture factor, which can be expressed as

$$C_f = \frac{P_{\text{PTO}}}{P_W \times D}, \tag{9}$$

where P_{PTO} is the power absorbed by the PTO system of the WEC which equals P_{total} here, P_W is the incident wave power and D is the physics width of the WEC. However, the definition of capture factor C_f to some extent as it is defined only in relation to the total absorbed power and does not sufficiently represent the difference of absorbed power along each PTO axis. Mode capture ratio $C_{\gamma}, C_{\theta}, C_{z}$ accounting for different PTO axes are defined as:

$$C_{\gamma} = \frac{P_{\gamma}}{P_{\text{total}}},\ C_{\theta} = \frac{P_{\theta}}{P_{\text{total}}},\ C_{z} = \frac{P_{z}}{P_{\text{total}}} \tag{10}$$

2.2 | Numerical model description

Developed to analyze the wave interaction of marine structures and ships, the BEM based numerical modelling software AQWA provides an engineering toolset for the investigation of the effects of waves on the renewable energy systems, especially the wave energy conversion devices. The relatively high efficiency in computation and low hardware requirements make the further optimization work of WECs possible. The simulations on power absorption performance of all the single and multi-axis WECs mentioned above are carried out with AQWA. The specific simulation settings are as follows.

2.2.1 | Simulation configuration

There are three steps to build a numerical model in AQWA. At first, the geometry of the WEC (includes several parts) is meshed to create non-diffracting and diffracting elements, respectively, and the simulation parameters need to be fully defined. It should be noted that the 64-bit version of the AQWA solver is limited to 40,000 elements, of which the diffracting elements should not be greater than 30,000. The models are illustrated with their surfaces meshed for hydrodynamic analysis, in Figure 3. There are four components composing of the models which are labelled components 1, 2, 3 and 4, respectively. The multi-axis WEC model consists of components 1, 2, 3 and 4. The single translation-axis WEC model consists of component 3 and 4. The single rotation-axis model consists of component 2, 3 and 4. It should be noted that component 3 is fixed in place in single translation-axis WEC model, as well as the component 2 in single rotation-axis WEC model. Furthermore, component 3 is kept in single rotation-axis WEC model such that the value of the pitching moment of inertia equals that of the multi-axis WEC model and fixed on component 4 to limit the relative translation motion between component 3 and 4. The physical properties of the components and meshing configuration are listed in Table 1, with their values and units.

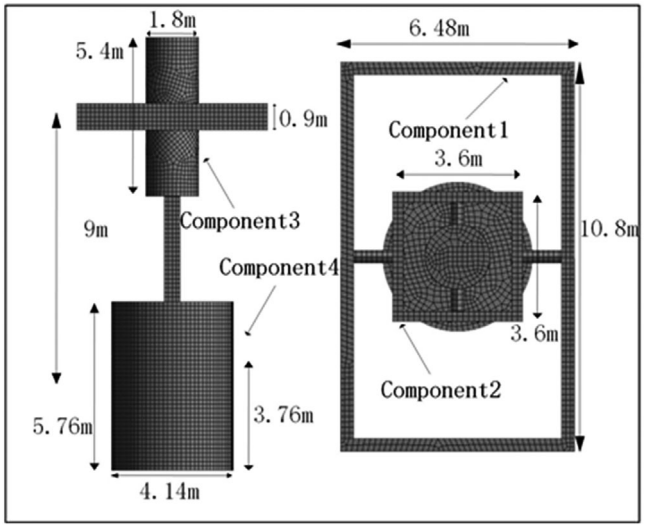

FIGURE 3 The mesh of the multi-axis WEC

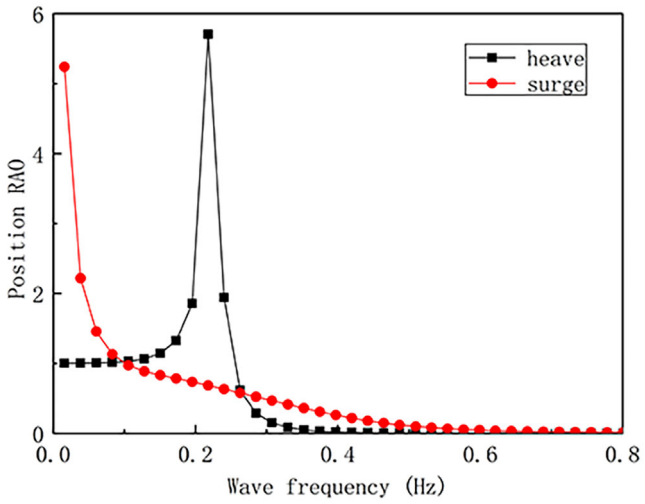

FIGURE 4 The position RAO of the buoy without multi-axis PTO system

In the second step, the analysis settings were established. First, the AQWA solver was used to solve the wave interaction of the parts containing diffracting elements in the frequency domain. A total of 50 frequency ranging from 0 to 1 Hz were calculated while the wave directions varied from 0° to 360° with an interval 15°. The velocities potentials were first calculated and the hydrodynamic coefficients, including the response amplitude operators, the diffraction forces, the radiation forces and the added mass were obtained. The frequency-domain results are shown in Figure 4. The response amplitude operator (RAO) in heave and surge of the cylindrical buoy without

TABLE 1 Physical properties of the components

		Component 1	Component 2	Component 3	Component 4
Dimensions	Length (m)	10.8	3.6	-	-
	Width (m)	6.48	3.6	-	-
	Height/draught (m)	0.9	0.9	5.4	5.76/3.76
	Diameter (m)	-	-	1.8	4.14
Connection type	Multi-axis WEC	Fixed	Hinged	Hinged	Free to move
	Single translation-axis WEC	-	-	Fixed	Single translation-axis
	Single rotation-axis WEC	-	Fixed	Hinged	Single rotation-axis

connecting to the multi-axis PTO system was obtained. It can be seen that the nature frequency of the buoy in heave was around 0.2 Hz. As can be seen in the follow-up simulation results, there will be significant differences between the motion responses of the buoy with and without multi-axis PTO system. Subsequently, based on the results obtained in frequency domain, the wave interaction of WEC models was solved in the time domain. The waves can be regular or irregular. Each simulation runs 200 s with a constant time step set as 0.01 s. For each time step in a simulation, the dynamic equation of motion was solved and the position and velocity of each part in the models was computed. As the wetted surfaces of the model vary significantly during a simulation, the hydrostatic and the Froude–Krylov forces were non-linear and calculated for each time step. The radiation force was calculated as the sum of the impulse response function convolution and the inertia force due to the added mass at infinite frequency was calculated.

2.2.2 | Waves

Once the numerical models were built and the parameters were determined, the characteristics of the power absorption performance of the multi-axis WEC with optimized linear PTO damping was examined for a broad range of regular wave conditions. Regular waves were characterized by their wave period (T) and wave height (H). More specifically, a total of 77 simulations were carried out under different wave conditions which are the combination between $T = 3, 3.2, 3.4, 3.6, 3.8, 4, 4.2, 4.4, 4.6, 4.8, 5$ s and $H = 0.2, 0.4, 0.6, 0.8, 1, 1.2$ and 1.6 m. For regular waves, the incident wave power P_W in $\mathrm{W}m^{-1}$ can be described as below:

$$P_W = \frac{1}{8}\rho g H^2 C_g, \tag{10}$$

where ρ, g and H present the wave density, gravity, wave height and C_g is the wave group velocity, which can be expressed as:

$$C_g = \frac{1}{2}\sqrt{\frac{g}{k}\tanh(kd)}\left[1 + \frac{2kd}{\sinh(2kd)}\right], \tag{11}$$

where k is wave number and d is water depth.

Subsequently, the multi-axis WEC is exposed to twelve different real sea states to test the ability to capture wave power in Zhejiang and Guangdong nearshore locations in East and South China Sea. A JONSWAP spectrum was used to simulate irregular waves characterized by two spectral parameters peak wave period (T_P) and the significant wave height (H_S), which can be expressed as

$$S_H(\omega) = 319.1\frac{H_s^2}{T_p^4\omega^5}\left\{-\frac{1948}{\left(T_p\omega\right)^4}3.3^{exp\left[-\frac{\left(0.159\omega T_p-1\right)^2}{2\sigma^2}\right]}\right\}. \tag{12}$$

2.2.3 | Numerical model validation

To validate the numerical model above with experimental data, a physical 1/10 scaled model of multi-axis WEC was tested in the wave flume of the Zhejiang University Ocean College, shown in Figure 5. The Froude similitude criterion was used to scale the experiment equipment and conditions. The dimensions of the wave tank are 25 m length, 0.7 m width and 0.7 m depth. The device was placed on the central line of the wave tank at a distance of 12.5 m from the wave-maker, as shown in Figure 6. The buoy's motion along each PTO axis is measured by displacement sensors. The wave condition of wave height 0.1 m and wave period 3 s is considered. Figure 7 compares the numerical and experimental results of the device's displacement along each PTO axis without PTO damping. It can be seen that the numerical and experimental results have a good agreement.

However, it should be noted that when the wave height is too high, angular displacement curve with smaller slope and reduced amplitude of the buoy would be found and evident difference was observed between the numerical and experimental results. It may due to undesired non-linear effects caused by the relatively larger wave height. Splashing and submergence can be observed during the experiment when the wave height is relatively high, which would slow the forward return rotation of the buoy. This non-linear phenomenon is very interesting and worth to be studied, but it's not the focus of this paper. In the follow-up simulation study, moderate waves are used to ensure the accuracy of the model.

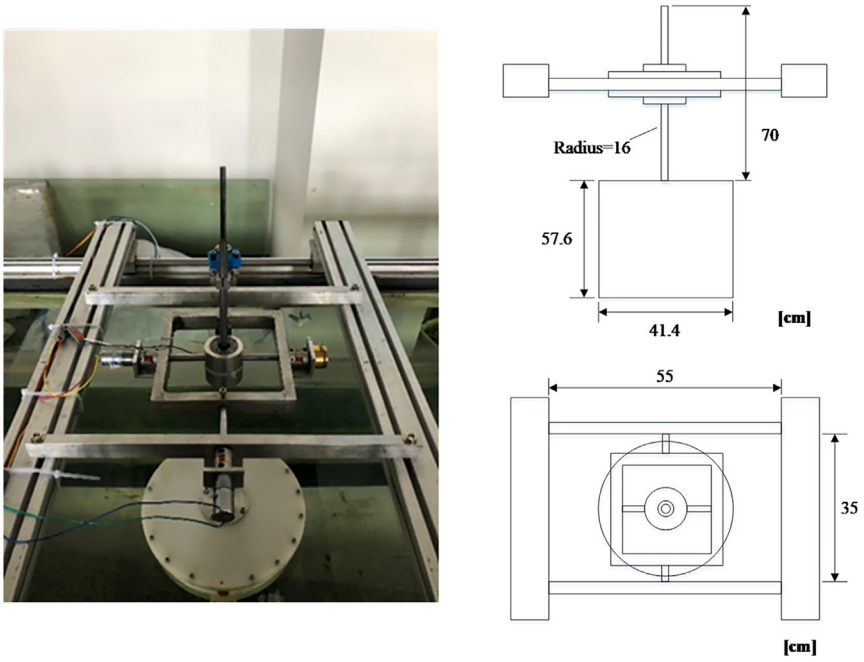

FIGURE 5 Physical model experiment

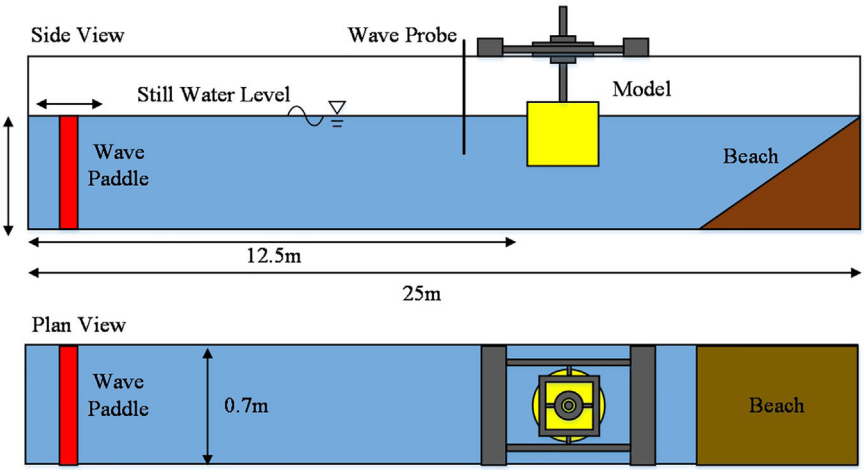

FIGURE 6 Experimental set-up in the wave flume

3 | RESULTS AND DISCUSSION

3.1 | Interactions between modes

The simulations for single-axis WECs aim to establish a reference point in order to investigate the effects of increasing number of DOFs on the power absorption capabilities of single-axis WECs. When allowing the WEC oscillates in more than one mode of motion, the interactions between modes will exist. As a result, both the total wave force acting on the buoy and the resulting amplitude of the motion in each mode differ from those of single-axis WECs. The interactions are investigated by analysing the translational response ratio and rotational response ratio defined as the ratio of the amplitude of translational or rotational motion to the wave height. Four simulation cases with the wave height 0.4, 0.8, 1.2 and 1.6 m are considered in this study. The incident wave angles are assumed to be 0° in all cases. The results of the translational and rotational response ratios of multi-axis and single-axis WECs versus the wave period are shown in Figure 8. In general, with lower wave height (H = 0.4, 0.8 and 1.2 m), both the translational and rotational response ratios of the buoy increases as the wave period increases, and approaches to the peak value at a certain period, and then decreases as the wave period continues to increase. The wave periods at which the translational and rotational response ratio in each mode reaches the highest point can be defined as the resonance periods in each mode, respectively. It is worth pointing out that there is a difference between the resonance periods in translation and rotation modes, indicating that the dominancy of the modes shifts from translation to rotational as the wave period increases. It can be seen that the translational response ratio in translational mode reaches

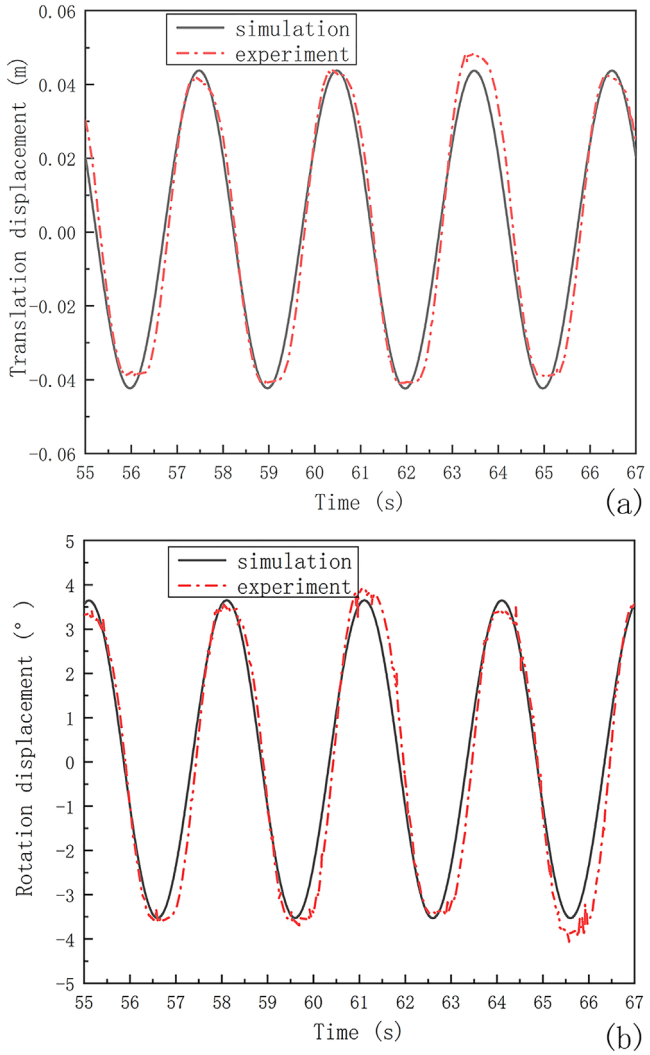

FIGURE 7 Validation with experimental data: (a) translation axis, (b) rotation axis

maximum at around 4.2 s. It is clear from the figure that the effects of wave heights on the peak values of translational and rotational response ratios are small. For the lower and higher wave periods, the differences between the translational and rotational response ratio curves of multi-axis WEC and single-axis ones are almost reduced to zero. Rotational response ratio curves show similar variation tendency to those presented in translation mode while the rotational response ratio reaches maximum at around 3.8 s in all cases.

One can see that in simulations with the highest wave height ($H = 1.6$ m), there is a depression in the translational response ratio curves close to the optimal frequency while the tendency of the rotational response ratio curves remains unchanged. It means that the value of translational response ratio no longer increases when the wave period approaches the resonance period. The phenomenon may be explained by the increasing tilt angle between the translation direction and the vertical axis caused by the increasing amplitude of rotational as the wave height increases. The angle is assumed small enough to be simplified as zero in the derivation of dynamic equations. The relatively large angle due to higher wave heights leads to the result that the additional resistance in horizontal direction starts to have an influence on the translation motion which cannot be neglected and thus the amplitude of translation is reduced.

The results of comparisons between translational and rotational response ratios of the multi-axis WEC and those of single-axis WECs are also seen in Figure 8. The results show that both the amplitudes of the motion of the multi-axis WEC in translation and rotation modes are smaller than those of single-axis WECs in all cases. The differences become more evident with the increasing wave height. The higher the wave height, the greater the impact.

The total wave force and moments acting on the multi-axis WEC and those acting on the single-axis WECs are shown in Figure 9. It indicates that for the multi-axis WEC, the interaction between modes plays a destructive role such that the total wave force acting on the buoy in each mode are reduced compared to those acting on single-axis WECs. The reduction in driving force can be an explanation for the reduction in translational and rotational response ratios mentioned above.

3.2 | Analysis on captured power and capture width ratio

Using the numerical model, the captured power matrices of the multi-axis WEC were computed. By dividing them by the incident wave power in each wave condition, the power capture efficiency of each device under each wave condition was derived. Results are reported in Figures 10 and 11.

Consider first the capture power matrices in Figure 10. One can see that the captured power increases as the wave period increases, and reaches its peak value at around the period 4s, and then decreases as the wave period continue to increase. The same tendency is found in the analysis of translational and rotational response ratios. An increase in the peak values can be found as the wave height increases, ranging from 0.8 kW to almost 10 kW. One can see that the multi-axis WEC is efficient in absorbing wave energy, being possible to reach 45% corresponding to waves of period 4 s and height 0.8 m. A clear relationship between the capture width ratio and the wave height is found: when the wave period is close to resonance period, the closer the wave height is to 0.8 m, the greater the capture width ratio is; when wave period is far away from the resonance period, the wave height has little effect on the efficiency. As for the relationship with the wave period, in general, the tendency is aligned with that of absorbed power. It is worth noticing that an increase in the captured power does not necessarily mean an increase in the capture width ratio. The reason is that the wave resource is larger as the wave height is greater, and thus more energy may be absorbed with a lower efficiency.

Figure 12 presents the comparison between the mean power absorbed by the multi-axis WEC and those of single-axis ones. The wave height is set as 0.8 m in all cases. The results show that the amount of the power absorbed by each mode of the multi-axis WEC in all wave conditions is less than that of the

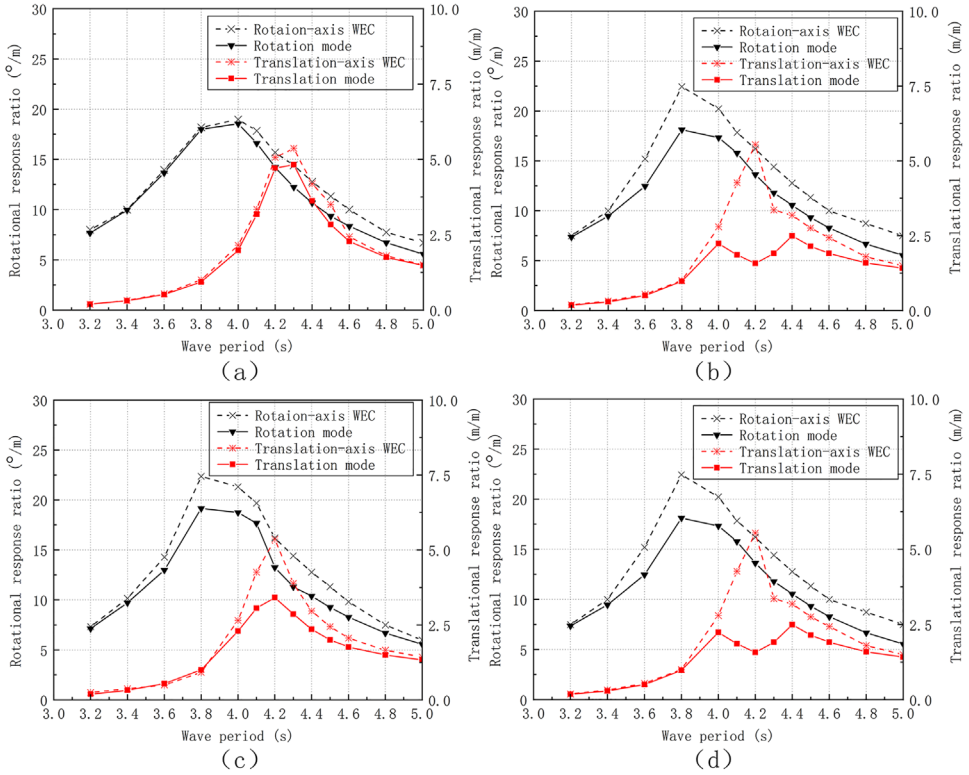

FIGURE 8 Translational and rotational response ratios versus wave period: (a) H = 0.4 m, (b) H = 0.8 m, (c) H = 1.2 m, (d) H = 1.6 m

corresponding single-axis WEC (translation mode versus single translation-axis WEC; rotation mode versus single rotation-axis WEC). It indicates that the increasing number of DOFs may bring a reduction in power absorption in each original mode of motion for a multi-axis WEC. However, one can see that the multi-axis WEC can absorb more wave power than any of single-axis devices at all wave frequencies. It shows that the multi-axis WEC has an advantage over the single-axis ones, in agreement with the results obtained from wave tank experiments.

3.3 | Studies on variations in mode capture ratio

For a typical point absorber WEC, the wave energy is usually converted to the kinetic energy of a buoy first, and then converted to usable electric energy through a hydraulic power system or an electrical generator. For the multi-axis WEC, the kinetic energy is captured independent from three different directions (one translation and two rotational axis). Although more wave energy can be absorbed, this introduces difficulties into the design of an efficient PTO system to convert simultaneously all the captured kinetic energy into usable energy. The absorbed energy in each mode differs in the peak value, the time of reaching at and staying at the peak. It is necessary to make this clear before any design work of PTO system has been done. To evaluate the performance in each mode, the mode capture ratios were calculated for each wave condition. In the following, we will show how the mode capture ratio in each mode varies with the wave frequency. In addition, the variation in the mode capture ratio with the incident angle is also presented and analysed. A 10 s time series of the instantaneous absorbed power with regular wave, as well as a 100 s time series with irregular wave, was demonstrated to shed light on how the absorbed power oscillations differs from mode to mode as shown in Figure 15.

Figure 13 shows the changes in the translation and rotation mode capture ratios over the wave period 3.5 to 4.5 s with the wave height 0.4, 0.8 and 1.2 m. The red bar represents the translation mode and the grey bar stands for the rotation mode. One can see from the figure that for a lower wave period, the power captured in rotation mode contributes more to the total captured power (the rotation mode capture ratio reaches up to 76%). This percentage remains basically steady until the wave period reaches around 3.8 s. From the wave period 3.8 s, the rotation mode capture ratio gradually decreases period by period while the percentage of the grey bar increases steadily. The translation mode capture ratio reaches the peak of 77% at around wave period 4.2 s. It starts to go down from the wave period 4.2 s at a smaller decreasing rate. One can see that the effects of wave height on the mode capture ratio are negligible. It is worth noting that the translation mode capture ratio equals the rotation mode capture ratio at around wave period 4 s. This can be defined as the optimal absorption situation for a multi- DOF system. For example, if a hydraulic PTO system were adopted, the equivalent power level in each mode provides

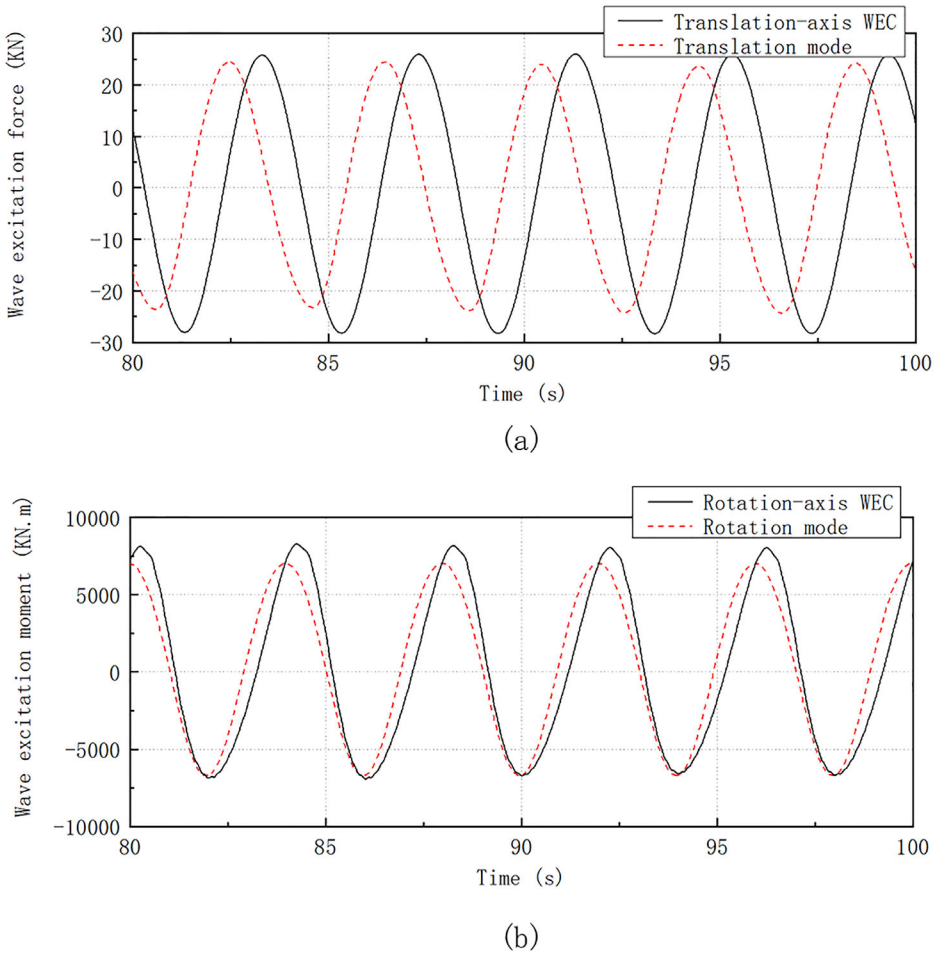

FIGURE 9 Differences in wave excitation force and moments between multi-axis and single-axis WECs: (a) wave excitation force, (b) wave excitation moment (in a regular wave with height 0.6 m and period 4 s)

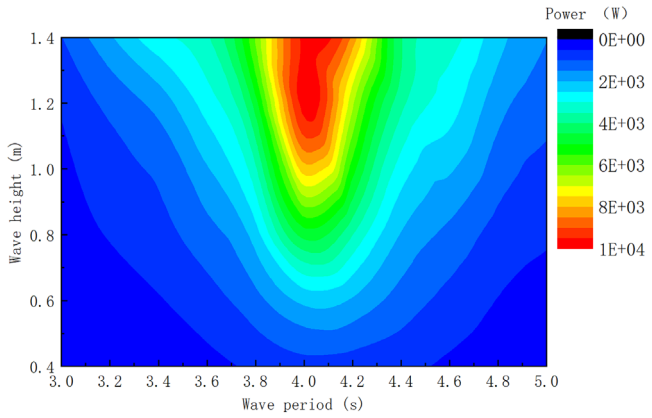

FIGURE 10 Absorbed power of the multi-axis WEC

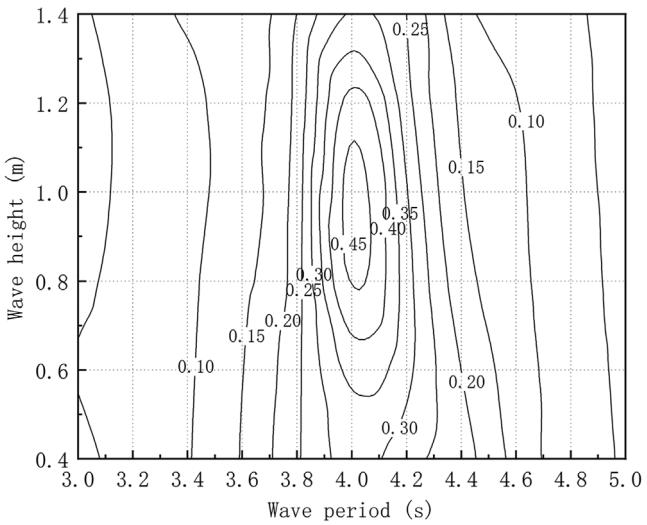

FIGURE 11 Power absorption efficiency of the multi-axis WEC

equivalent pressure and flow in every hydraulic branch which avoids the interference between modes. This is similar to the case in the large-scale array of WECs. The different hydraulic pressure of each device in the WEC field will interfere with each other resulting in the reduction of the efficiency of the wave energy conversion. One WEC can even become the load of the others [19]. One multi-axis WEC can be regarded as a point absorber WEC array consisting of three single-axis devices from the energy collection point of view, so that it is necessary to

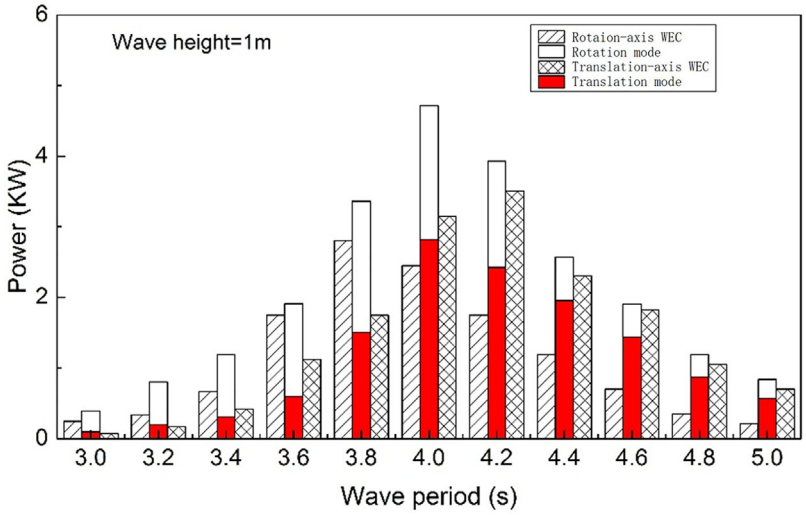

FIGURE 12 Comparison between multi-axis and single-axis WECs (wave height = 0.8 m)

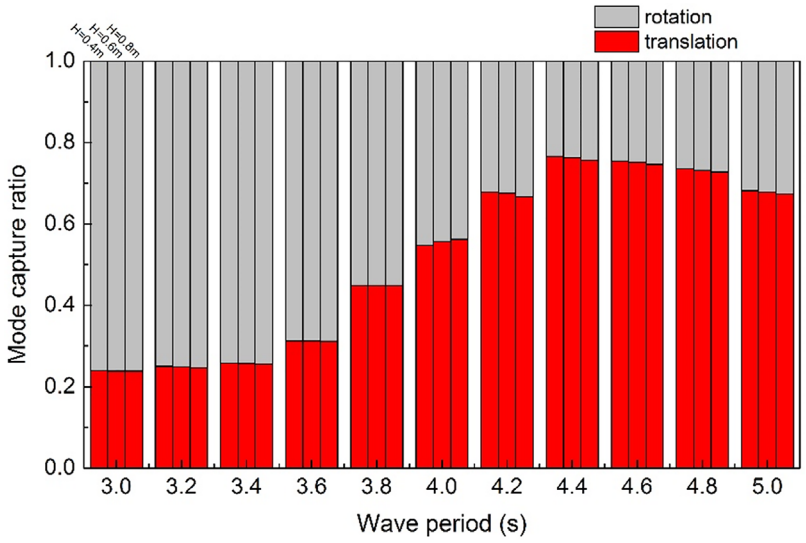

FIGURE 13 Variation in model capture ratios with wave period (H = 0.4, 0.6, 0.8 m)

ensure the difference between mode capture ratios in translation and rotation modes is minimal for absorbing more wave energy.

One should notice that not only the wave frequency varies during a long operation period, but also the direction of the waves is changing all the time. For single-axis WECs, the time-varying wave direction barely affects the single translation-axis device, but significantly influences the single rotation-axis device due to its fixed orientation of wave ward side. In present-day pitching WEC designs, in general, the orientation of the buoy of the WEC needs to be adjusted all the time, which reduces the applicability and conversion efficiency of pitching devices. The multi-axis WEC has advantages over the single-axis WECs. We defined the angle between the wave direction and the axis of rotational 1 as the incident angle. The effects of the incident angle of waves on the mode capture ratio are investigated, as shown in Figure 14. The value of the incident angle ranges from 0° to 90° with the interval of 15°. The wave heights are 0.6 m and the wave periods are set as 4 s in all cases such that the translation mode capture ratio nearly equals to 50%. It was observed that the translation mode capture ratio is slightly influenced by the incident angle, while the rotation mode capture ratio is significantly affected. This was to be expected as the wave excitation moment is decomposed into two components each of which drives two rotational motions respectively. The driving moment is varying with the incident angle, and thus the captured power is oscillatory too. It can be seen that the multi-axis WEC only operates in two modes under the wave conditions with the incident angle 0° and 90°.

Figure 15a shows an example of the instantaneous absorbed power by the multi-axis WEC. The instantaneous absorbed power is too oscillatory be sent directly to the grid and it is necessary to set a rated power for the PTO system. The settings of the rated power have a significant influence on the power absorption. In this example, we set the rated power as 7.5 kW for illustration purpose. The incident wave is regular with period 4 s and height 0.6 m. One can see that the instantaneous absorbed power in each mode is both going to zero twice per cycle and stays within the range between 0 and 22.5 kW. The absorbed power in translation mode varies with time

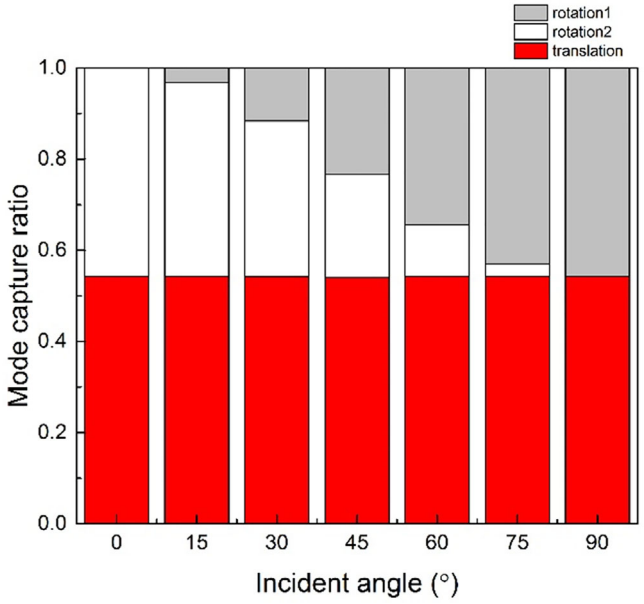

FIGURE 14 Variation in mode capture ratios with wave incident angle

TABLE 2 Mean spectral parameters of JONSWAP Spectral for the seven sea states in East and South China Sea

Location	Sea states	Mean Hs (m)	Mean Tp (s)
Zhejiang	Dajishan	0.6	2.3
	Shengshan	1.2	4.4
	Dongfushan	0.5	5.6
	Beiyushan	0.4	8.2
	Zhenhai	0.3	1.9
	Dachendao	1	5.3
	Nanjidao	1.1	4.9
Guangdong	Yunao	0.6	4.5
	Zhelang	1.1	4.5
	Luzhou	1	4.6
	Dongfang	0.8	3.6
	Xisha	1.4	3.8

sinusoidal reaching the local peak twice per circle and the difference between the values of the local peaks is small. One can see that the multi-axis WEC mainly absorbs wave power in the first half of the rotational movement and has a local peak greater than any of those in translation mode. These power absorption characteristics of multi-axis WEC mentioned above can also be observed in irregular wave condition shown in Figure 15b. We take the total instantaneous power of the multi-axis WEC as the power ultimately transmitted to the generator. It is equal to the sum of translation and rotational instantaneous power. It is known to all that the generator speed drops to zero when the absorbed power goes to zero if a single-axis WEC is deployed in the wave energy conversion system. On the opposite, as we can see from the figure, the total instantaneous power no longer goes to zero and stays within the range between 2.5 and 25 kW due to the phase difference between translation and rotational instantaneous power curves. The power absorbed in these two modes is delivered to the PTO system alternately such that their peaks staggered off. Moreover, when the rated power is set as 7.5 kW here, the period that the instantaneous total absorbed power exceeds the rated power has been extended compared to any of single-axis WECs. Therefore, it means that a more stable and continuous input energy are transmitted to the generator; in other words, power shocks or downtime problems can be reduced significantly.

4 | APPLICATION TO REAL SEA STATES

Moderate waves are frequently observed along the coast of China in which the wave energy reserves are at available level. The annual wave power density observed in East and South China Sea are generally greater than 2 kW/m [20], which is very promising and suitable for the development and utilization of wave energy. In this section, the power absorption performance of the multi-axis WEC is investigated considering twelve different sea states observed in East and South China Sea, as shown in Figure 16. The parameters of wave energy spectrum used in the modelling of sea states were derived from the wave data recorded by the China offshore Marine Research which were conducted between 1984 and 2017 [21]. A JONSWAP spectral shape with the different values of the spectral significant wave height and the peak wave period (Table 2) is used to simulate all the selected wave conditions.

In the East China Sea off the coast of Zhejiang Province, the sea state Shengshan is the most energetic one giving the highest mean wave height (1.2 m). In general, the higher the wave height, the more energetic the wave climate is. The sea state Zhenhai is the one with the lowest wave energy due to the lowest wave height (0.3 m) and the lowest peak period (1.9 s) existing in this area. The sea state Dajishan is characterized by relatively low wave heights (higher than 0.5 m, but lower than 1 m). The sea state Dongfushan, which is the farthest location from the coastline, is also characterized by low wave heights. The sea state Beiyushan has the highest period (8.2 s) with low wave heights. The sea states Nanjidao and Dachen are the other two locations with the wave heights over 1 m and their peak periods is close.

In the South China Sea off the coast of Guangdong Province, the sea state Xisha is the farthest from the coastline and has the highest wave height (1.4 m), which means the most energetic location. The sea state Dongfang and Yunao are the ones with the lower wave energy due to the lower wave height. The sea state Luzhou has the highest period (8.2 s) with moderate wave heights. In the South China Sea, the difference between wave periods of all the sea states is not as significant as in the East China Sea, ranging from 3.5 to 4.5 s.

The influence on the performance of the multi-axis WEC in relation to the difference between the sea states is investigated by means of the parameters mean absorbed power, power

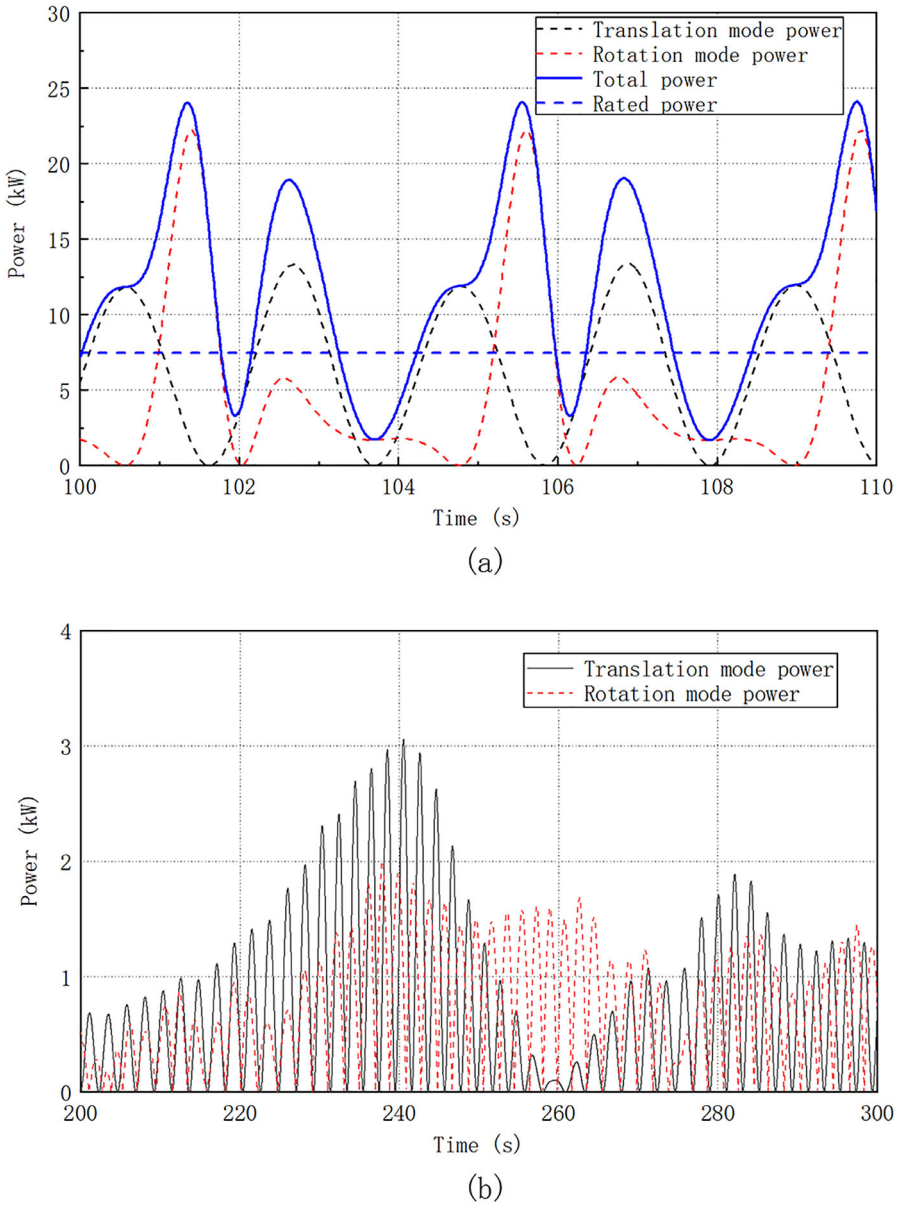

FIGURE 15 Instantaneous absorbed power in translation and rotation modes: (a) regular wave (H = 0.6 m, T = 4 s), (b) irregular wave condition (Hs = 0.6 m, Tp = 4 s)

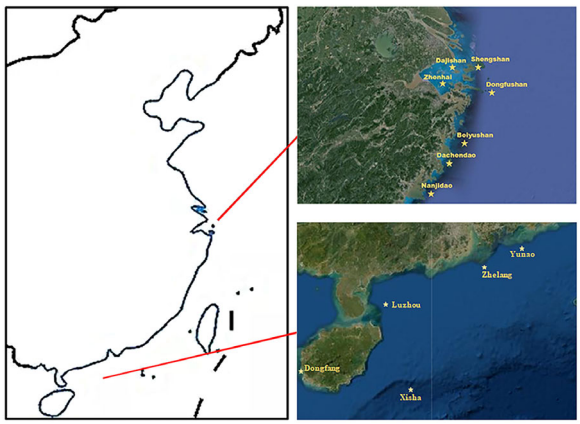

FIGURE 16 The 12 sea states in East and South China Sea

absorption efficiency aligned with the foremost concerns in the analysis with regular waves. Figure 17 shows the results obtained for mean absorbed power and power absorption efficiency. Overall, remarkable differences in terms of the absorbed power (from 0.1 to 5 kW) and efficiency (from 4% to 29%) can be found between sea states. This figure illustrates that Shengshan is the optimum deployment location among all the sea states in the East and South China Sea where the most wave energy can be harvested (5 kW) by the multi-axis WEC. For the sea state Zhelang and Luzhou in South China Sea, the power absorption performance of the multi-axis WEC is also satisfactory with absorbed power close to 5 kW. However, for the sea state Dongfushan with significantly lower wave height than those in sea states Dachen and Nanji, the multi-axis WEC has a considerable efficiency exceeding values of 10%.

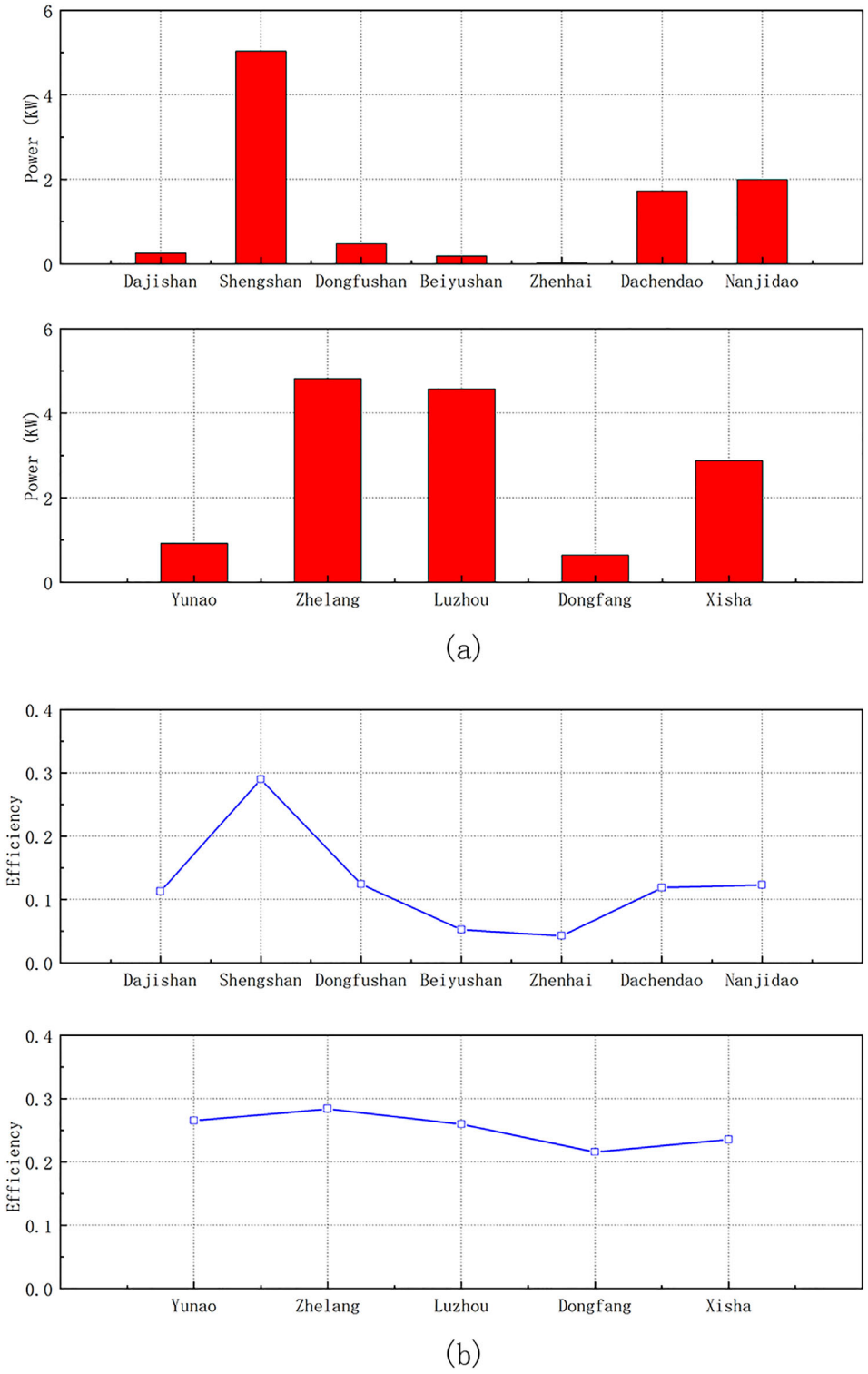

FIGURE 17 The absorbed power and efficiency in each sea state: (a) mean absorber power (b) efficiency

This fact can be explained by their peak periods are close to each other. Unsatisfactory performance is also found in sea states Yunao and Dongfang due to their lower wave height. The most disappointing result is that the multi-axis WEC does not perform well at the most energetic sea state Xisha in South China Sea. The results obtained also show considerable differences between the amount of the absorbed power in the sea states Shengshan and those in sea states Dachen and Nanji.

For the monthly case, the locations where the multi-axis WEC performs best were used to assess in detail the performance of multi-axis WEC on a monthly basis, as shown in

TABLE 3 Monthly mean spectral parameters of JONSWAP Spectral for the sea states Shengshan and Zhelang

	month	1	2	3	4	5	6	7	8	9	10	11	12
Shengshan	Hs	1.1	1.1	1.0	1.0	0.9	0.9	1.1	1.0	1.0	1.1	1.0	1.0
	Tp	4.9	5.0	4.7	5.0	4.6	5.0	5.4	5.0	4.9	5.0	4.8	4.7
Zhelang	Hs	1.2	1.2	1.2	1.0	1.0	1.0	1.0	1.0	1.1	1.4	1.4	1.3
	Tp	3.8	3.9	3.9	3.8	3.7	3.8	3.8	3.7	3.8	3.9	4.0	3.9

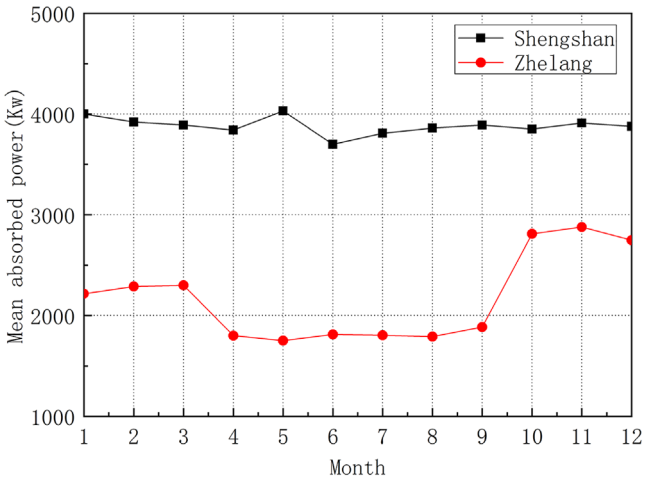

FIGURE 18 Monthly mean absorbed power of sea state Shengshan and Zhelang

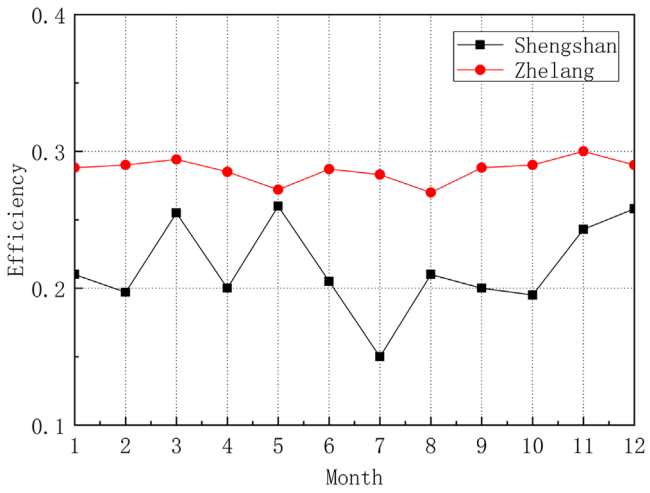

FIGURE 19 Monthly efficiency of sea state Shengshan and Zhelang

Table 3. In general, differences of wave sources were found between the months. This fact is especially relevant for wave period at sea state Shengshan, where the wave period presents random variations ranging from 4.6 to 5.0 s. Conversely, at sea state Shengshan, the wave heights are quite homogenous with months, and maintain at about 1 m. With respect to the sea state Zhelang, minor differences were found with the wave period, where the wave height changes significantly with the month. The monthly variations of mean absorbed power and efficiency are represented in Figures 18 and 19. Overall, different behaviour was found for the sea states. For sea state Zhelang, the mean absorbed power with the winter months (from October to March) achieves relatively higher values. On the contrary, the mean absorbed power for sea state Shengshan are quite not related to seasonal changes. In addition, efficiency increases for sea state Zhelang reaching values close to 0.32 in November. For sea state Shengshan, the efficiency presents a noticeable monthly variation, decreasing around 5% from the highest to the lowest month.

Based on the analysis of captured power and efficiency in each sea state, some suggestions on the application of the multi-axis WEC in Zhejiang and Guangdong nearshore locations in East and South China Sea can be given as follows. For the more energetic sea states with different peak periods, the scale of the system is necessary to be altered to adjust the resonance period of the WEC to match the peak period. Single multi-axis WEC is not recommended to be deployed in the sea states such like Beiyushan, Zhenhai and Yunao with lower wave energy. Reducing the size of the WEC and deploying it in an array can be an alternative choice to absorb wave power in these less energetic locations, like [22]. It can be concluded that the current design of the multi-axis WEC cannot be optimal simultaneously for all the sea states in East and South China Sea. Future works are recommended to adapt the proposed WEC for different wave conditions by adjusting the design concepts, for example, altering the scale of the system or optimizing the geometry of the buoy.

5 | CONCLUSION

Here, the multi-axis WEC with a cylindrical buoy was considered and simulated with regular waves and real sea states using numerical models built in AQWA. Based on obtained results, the following conclusions were drawn.

For the multi-axis WEC under regular wave conditions, the captured power differs a lot, from 0.1 kW with the least energetic wave condition up to 10 kw for the 4s wave period with the highest wave height. In terms of capture width ratio, the multi-axis WEC can absorb more than 45% of the incident wave power. Compared to the single-axis WECs, no matter the single translation-axis or the single rotation-axis devices, the multi-axis WEC captures less power in the corresponding mode but absorb more wave energy in total, and it performs well in a wider band of wave frequency than any kind of single-axis devices.

For the lower wave period, the multi-axis WEC behaves more like a single rotation-axis device. As the wave period increases, the rotation mode dominant motion shifts to the translation mode dominant motion almost linearly. When the wave period reaches 4 s, the power captured in translation mode almost equals that in rotation mode. For the higher wave period, the multi-axis WEC behaves more like a single translation-axis device. It was observed that the incident angle slightly influences the translation mode capture ratio; on the opposite, it significantly affects the rotation mode capture ratio.

As for the simulations in real sea states in East and South China Sea, the results indicate that the multi-axis WEC can absorb up to 5 kW and the capture width ratio can reach up to 29%. It shows that Shengshan and Zhelang is the optimum deployment location where the most wave energy can be harvested by the multi-axis WEC.

We believe that the numerical modelling of the multi-axis WEC is very useful to investigate the characteristics of the power absorption performance of this device. This analysis can hopefully help in choosing the right site and resizing the device for the application of the multi-axis WEC in Zhejiang and Guangdong nearshore in East and South China Sea. This paper leaves some interesting open questions, which are a topic for further research, including the effects of supporting base or mooring system, control strategies and geometry optimization due to specific sea state.

CONFLICT OF INTEREST

There are no conflicts of interest

PERMISSION TO REPRODUCE MATERIALS FROM OTHER SOURCES

None.

ACKNOWLEDGEMENTS

The study is supported by National Key R&D Program of China (Grant No. 2018YFB1501900 and 2018YFB1501904), the Key Research and Development Program of Zhejiang Province (Grant No. 2021C03182), the National Natural Science Foundation of China (Grant No. 51879233), Natural Science Foundation of Zhejiang Province (Grant No. LHY20E090001), Bureau of Science and Technology of Zhoushan (Grant No. 2019C81036 and 2021C81001), and the Fundamental Research Funds for the Central Universities. The authors are grateful for the provision of financial support. The computational resources in the HPC Center of Zhejiang University (Zhoushan Campus) are also acknowledged.

DATA AVAILABILITY STATEMENT

The raw/processed data required to reproduce these findings cannot be shared at this time as the data also forms part of an ongoing study.

ORCID

Ming Tan https://orcid.org/0000-0001-7209-4083

REFERENCES

1. Falcão António, F. de O.: Wave energy utilization: A review of the technologies. Renewable Sustainable Energy Rev. 14(3), 899–918 (2010). http://doi.org/10.1016/j.rser.2009.11.003
2. Budal, K., et al.: The Norwegian wave-power buoy project. Proceedings of the 2nd International Symposium on Wave Energy Utilization, pp. 323–344 (1982)
3. Weber, J., et al.: Wavebob–research & development network and tools in the context of systems engineering. Proceedings of the 8th European Wave and Tidal Energy Conference, pp. 416–420 (2009)
4. Powerbuoy: Ocean Power Technologies (2016) http://www.oceanpowertechnologies.com/powerbuoytechnology
5. AWS Ocean: Archimedes Waveswing Submerged Wave Power Buoy (2016). http://awsocean.com/technology/archimedeswaveswing-submerged-wave-power-buoy
6. McCabe, A.P., Bradshaw, A., Meadowcroft, J.A.C., Aggidis, G.: Developments in the design of the PS Frog Mk 5 wave energy converter. Renewable Energy 31(2), 141–151 (2006). http://doi.org/10.1016/j.renene.2005.08.013
7. Zhang, D., George, A., Wang, Y., Gu, X., Li, W., Chen, Y.: Wave tank experiments on the power capture of a multi-axis wave energy converter. J. Mar. Sci. Technol. 20(3), 520–529 (2015). http://doi.org/10.1007/s00773-015-0306-5
8. Zhang, D., Aggidis, G., Wang, Y., Mccabe, A., Li, W.: Experimental results from wave tank trials of a multi-axis wave energy converter. Appl. Phys. Lett. 103(10), 103901 (2013). http://doi.org/10.1063/1.4820435
9. Yavuz, H.: On control of a pitching and surging wave energy converter. Int. J. Green Energy 8(5), 555–584 (2011). http://doi.org/10.1080/15435075.2011.576291
10. de Andrés, A.D., Guanche, R., Armesto, J.A., del Jesus, F., Vidal, C., Losada, I.J.: Time domain model for a two-body heave converter: Model and applications. Ocean Eng. 72, 116–123 (2013). http://doi.org/10.1016/j.oceaneng.2013.06.019
11. Pastor, J., Liu, Y.: Power absorption modeling and optimization of a point absorbing wave energy converter using numerical method. J. Energy Resources Technology 136(2), (2014). http://doi.org/10.1115/1.4027409
12. Ning, D., Shi, J., Zou, Q., Teng, B.: Investigation of hydrodynamic performance of an OWC (oscillating water column) wave energy device using a fully nonlinear HOBEM (higher-order boundary element method). Energy 83, 177–188 (2015). http://doi.org/10.1016/j.energy.2015.02.012
13. López, M., Taveira-Pinto, F., Rosa-Santos, P.: Influence of the power take-off characteristics on the performance of CECO wave energy converter. Energy 120, 686–697 (2017). http://doi.org/10.1016/j.energy.2016.11.121
14. López, M., Taveira-Pinto, F., Rosa-Santos, P.: Numerical modelling of the CECO wave energy converter. Renewable Energy 113, 202–210 (2017). http://doi.org/10.1016/j.renene.2017.05.066
15. Falcão, A.F. de O., Rodrigues, R.J.A.: Stochastic modelling of OWC wave power plant performance. Appl. Ocean Res. 24(2), 59–71 (2002). http://doi.org/10.1016/s0141-1187(02)00022-6
16. Babarit, A., Duclos, G., Clément, A.H.: Comparison of latching control strategies for a heaving wave energy device in random sea. Appl. Ocean Res. 26(5), 227–238 (2004). http://doi.org/10.1016/j.apor.2005.05.003
17. Falcão António, F. de O.: Phase control through load control of oscillating-body wave energy converters with hydraulic PTO system. Ocean Eng. 35(3-4), 358–366 (2008). http://doi.org/10.1016/j.oceaneng.2007.10.005
18. Gomes, R.P.F., Lopes, M.F.P., Henriques, J.C.C., Gato, L.M.C., Falcão, A.F.O.: The dynamics and power extraction of bottom-hinged plate wave energy converters in regular and irregular waves. Ocean Eng. 96, 86–99 (2015). http://doi.org/10.1016/j.oceaneng.2014.12.024
19. Lin, Y., Bao, J., Liu, H., Li, W., Tu, L., Zhang, D.: Review of hydraulic transmission technologies for wave power generation. Renewable Sustainable Energy Rev. 50, 194–203 (2015). http://doi.org/10.1016/j.rser.2015.04.141
20. Luo, X., et al.: Analysis on the Characteristics of the Resource of Marine Energy in Key Offshore Area in China. Ocean Press, Beijing, China (2017)

21. Han, J., et al.: China Offshore Ocean: Marine Renewable Energy. Ocean Press, Beijing, China (2015)
22. Liu, Z., Qu, N., Han, Z., Zhang, J., Zhang, S., Li, M., Shi, H.: Study on energy conversion and storage system for a prototype buoys-array wave energy converter. Energy for Sustainable Development 34, 100–110 (2016). http://doi.org/10.1016/j.esd.2016.07.004

How to cite this article: Tan, M., et al.: Power absorption modelling and analysis of a multi-axis wave energy converter. IET Renew. Power Gener. 15:3368–3384 (2021) https://doi.org/10.1049/rpg2.12277.